LHCb Collaboration LHCb 2002-028 TRIG
April 26, 2002

Tuning the Super Level 1 algorithm to the VELO-TDR geometry

N. Tuning
CERN, CH-1211 Geneva 23, Switzerland

Abstract

This note describes an update of the Super-Level 1 trigger algorithm. The SL1 trigger algorithm finds tracks and secondary vertices in the vertex detector and matches tracks to muons, electrons and hadrons, found at the previous trigger level (L0). The original algorithm was tuned on the detector geometry of LHCb as described in the Technical Proposal, whereas the results presented here, are obtained using the detector geometry as described in the various Technical Design Reports.

1 Introduction

This note describes an update of the Super-Level 1 trigger algorithm (SL1) [1]. The SL1 trigger algorithm finds tracks and secondary vertices in the vertex locator (VELO) [2] and matches tracks to muons, electrons and hadrons found at the first trigger level, L0. The original algorithm was tuned on the detector geometry of LHCb as described in the Technical Proposal (TP) [3], whereas this results presented here, are obtained using the detector geometry as described in the various Technical Design Reports (TDR) [4, 5, 6].

Studies are ongoing to install a tracking detector (TT1) between the RICH1 and the magnet and use its information in the trigger Level 1 (L1). With the magnetic shielding plates removed, this detector can provide momentum information for each track, with potentially large improvements in the L1 performance. These studies are not part of this note. The matching of VELO tracks to L0 objects remains however of large interest for the final L1 decision.

The original SL1 algorithm and the present studies were both tuned under the following conditions:

- Tuned Pythia 6.134
- $\mathcal{L} = 2 \cdot 10^{32}$ cm^{-2}s^{-1}.
- All events passed L0 decision + L0 pile-up veto.
- Signal events passed tightest AXSEL selection.
- Signal events are rejected if > 1 MC vertex.

The differences between the TP and TDR algorithms are listed in Table 1.

TP:	TDR:
dBase v228r1	dBase v239
X/X_0, VELO vacuum vessel = 7.5%	X/X_0, VELO vacuum vessel = 19% [7]
17 VELO stations	25 VELO stations
top/bottom VELO halves	left/right VELO halves
$90^o/45^o$ VELO sectors (put in by hand)	$60^o/30^o$ VELO sectors
smaller/larger inner/outer CAL cells	larger/smaller inner/outer CAL cells
wider MUON pads	MUON pads more rectangular
SICB v235r1 reconstruction	Brunel v5r1 reconstruction
Fortran L1 tracking	C^{++} L1 tracking [8]
Fortran L0 information	C^{++} L0 information

Table 1: *The different conditions for the SL1 algorithm for the TP and the TDR setup.*

The data used here were simulated using database v239 of the LHCb detector, and were reconstructed with Brunel v5r1. The complete data sets are the "high-priority" data sets [9] listed in Table 2 [1].

[1] When these data were produced the two channels $B_d^0 \to D^{*-}\pi^+$ and $B_s^0 \to K^+K^-$ were not yet defined to be high-priority channels, and therefore no data were generated for these channels.

Event type		On tape	L0	L0+AXS	No Vtx	Clus	Tracks (single)	1 MC Vtx	Total
61	Min.Bias	100000	7.0%	(x)	6.0%	0.5%	-	100%	6502
360000	$B_d^0 \to X$ (in 4π)	10000	21.8%	(x)	4.0%	0.5%	-	56%	1163
412100	$B_d^0 \to \pi^+\pi^-$	23500	40.8%	3.89% (2)	3.7%	0.5%	(B) 80.9% (90%)	60%	400
411300	$B_d^0 \to J/\Psi(\mu^+\mu^-)K_S$	19500	70.0%	1.44% (2)	4.6%	0.7%	(Ψ) 85.3% (92%)	52%	118
412800	$B_d^0 \to \pi^+\pi^-\pi^0$	25000	36.9%	0.13% (1)	3.1%	0.0%	-	67%	18
414500	$B_d^0 \to \overline{D}^0 K^{0*}$	17500	38.0%	0.28% (2)	4.1%	0.0%	(D) 77.3% (88%)	65%	22
613400	$B_s^0 \to D_s^{\pm} K^{\mp}$	19500	37.4%	1.05% (2)	1.5%	1.0%	(D) 63.2% (86%)	61%	70
411400	$B_d^0 \to J/\Psi(e^+e^-)K_S$	22000	32.5%	5.97% (0)	5.5%	0.3%	(Ψ) 79.4% (89%)	60%	485
412500	$B_d^0 \to K^{0*}\gamma$	25500	31.4%	7.87% (0)	4.3%	0.4%	-	60%	832

Table 2: *The data sets used in this analysis are listed. The fraction of events selected at L0 and by AXSEL are given in column 4 and 5 respectively. The highest available AXSEL selection level is applied and is shown in brackets. The fraction of rejected events due to the reconstructed vertex requirement is given in column 6. Column 7 shows the fraction of events with more than 128 R-clusters in a 60º sector. Additional event selection steps are shown in columns 8 and 9. For five decay channels, the decay products of the resonance in brackets are required to be reconstructed in the VELO. The corresponding single 3d-track finding efficiency is shown in brackets. Column 9 shows the fraction of events with one primary vertex, as generated by the Monte Carlo. The last column shows the total number of events after full event selection.*

The HCAL energy was miscalibrated by +40% (corrected in Brunel v9.0) and was scaled down by hand. The L0 decision is repeated after rescaling the HCAL energy scale, using the parameters from Table 3. The resulting output rate of the L0 then corresponds to the design rate [10].

Note that the AXSEL selection is not tuned to this particular detector geometry [11]. In the tracking program for the trigger, the primary vertex is reconstructed using the 2d tracks. If there are less than 10 2d-track pairs in the range $-10 < Z < 10$ cm or less than 10 2d-track pairs around ± 0.14 cm around this primary vertex, then the primary vertex is not reconstructed [8]. The fraction of events without a primary vertex is shown in Table 2. Particles produced at very wide angles (close to 90^o) may hit many R-strips in one silicon sensor. If the number of clusters exceeds 128 [12, 13], then the event is not reconstructed. Rejecting these events should not bias the event sample, since the vertex distribution is equal for underlying events.

L0 muon P_T cut	0.55 GeV
L0 electron P_T cut	2.72 GeV
L0 gamma P_T cut	5.14 GeV
L0 hadron P_T cut	**3.10 GeV**
L0 sum P_T $\mu\mu$ cut	5.90 GeV
L0 min ΣE_T cut	5 GeV

Table 3: *The settings used for the L0 decision are listed. These values correspond approximately to a bandwidth division of 6:2:1:0.1 for hadron:muon:electron:gamma [10]. However, the L0 hadron P_T cut is lowered from 3.8 to 3.1 GeV.*

In addition, decay particles of five decay channels are required to be found by the 3d track reconstruction in the L1 tracking. The tracking efficiency is thus not folded in to the trigger efficiency. The single track finding efficiency is also given in Table 2.

Signal events with multiple interactions are rejected as well, selecting approximately 60% of the events.

2 Structure of Super-Level 1

The structure of the Super-Level 1 algorithm is listed below and is schematically shown in Fig. 1. The details concerning the Super-Level 1 algorithm are described elsewhere [1].

1) 2d-tracks in the rz-projection are constructed.
2) The primary vertex is constructed.
3) A b-probability is assigned to each 2d-track, mainly based on the impact parameter.
4) 2d-tracks are matched to L0 candidates.
5) Matched 2d-tracks or 2d-tracks with large b-probability are reconstructed in 3d.
6) 3d-tracks are matched to L0 candidates.
7) Five b-probabilities are assigned to each matched 3d-track.
8) Matched or unmatched 3d tracks are selected.
9) Two-track vertices (ttv) are constructed.
10) Six b-probabilities are assigned to each two-track vertex.
11) Three b-probabilities are assigned to each event.
12) The maximum of the 3 event probabilities is used for the event decision.

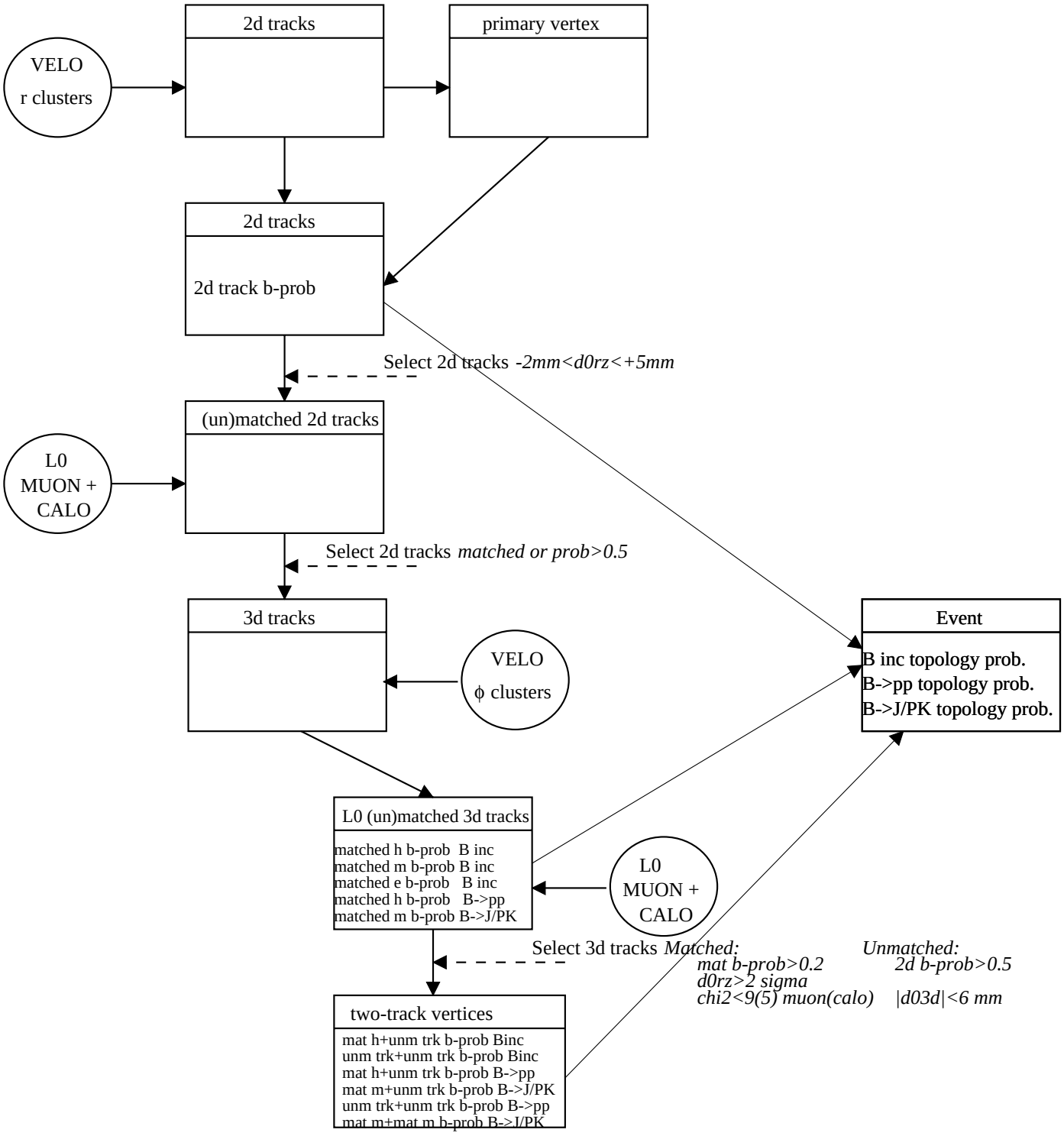

Figure 1: *The structure of SL1 is schematically shown. The various b-probabilities assigned in each step are indicated in the boxes.*

3 2d Impact parameter

The L1 trigger strategy relies on the measurement of detached vertices, originating from B-decays. The precision of the impact parameter measurement determines how precise secondary vertices are found. For low momentum tracks ($p_T \lesssim 1$ GeV) the uncertainty on the impact parameter is fully determined by multiple scattering [4]. The more material a low momentum particle traverses, the more the particle will multiple scatter and consequently mimic a high impact parameter B-decay product.

In Fig. 2 the 2d impact parameter distributions are shown for three detector geometries. The TDR geometry has most dead material between the primary vertex and the second measured point of the VELO, see Table 4. This is reflected in a broader impact parameter distribution for all 2d-tracks.

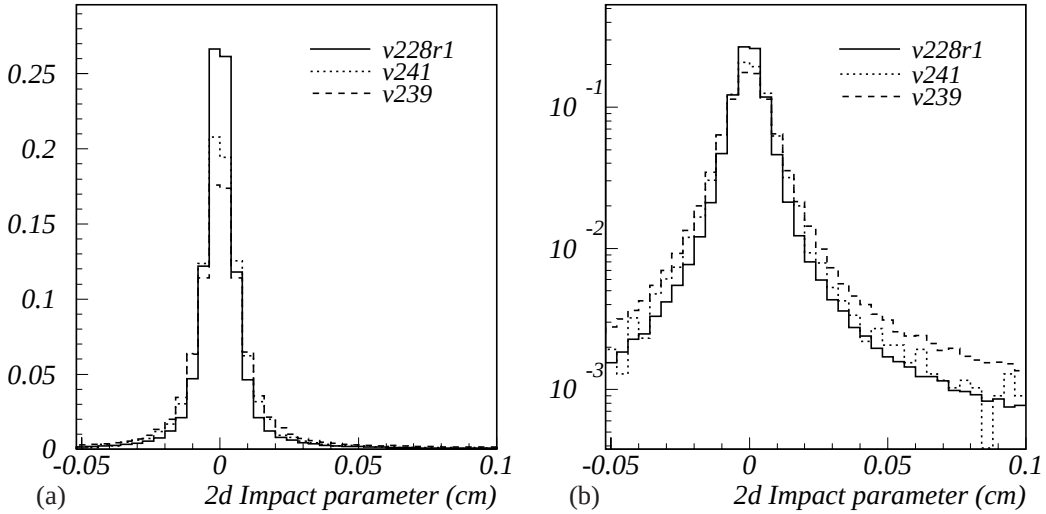

Figure 2: *(a) The normalised 2d impact parameter distributions for all 2d tracks are shown for three different LHCb detector geometries. (b) The impact parameter distributions are shown on a log scale.*

In the SL1 algorithm the impact parameter is first calculated using 2d-tracks. Precious time is gained by reconstructing only those 2d-tracks in 3d, that have a significantly large impact parameter. The importance of the impact parameter justifies the explicit calculation below. Consider the primary vertex at the centre of the VELO, at $X = Y = 0$.

Detector	dBase	RF foil	Si	X/X_0 (VELO+vacuum vessel)
TP	v228r1	100 μm	150 μm	7.5%
TDR	v239	250 μm	300 μm	19%
Light	v241	100 μm	220 μm	13.3%[2]

Table 4: *The thicknesses of the RF foil and the silicon sensors are given for three different geometries.* [2] *The X/X_0 for the light configuration is calculated assuming that the Si and RF foil contribute 6.1% and 6.9% respectively to the total amount of material [7]:* $X/X_0 = 0.19 - \frac{220}{300} \times 0.061 - \frac{100}{250} \times 0.069 = 0.133$

The 2d-tracks in the rz-plane are determined by three r clusters, called a triplet and are parametrised as $r = b + mz$ [2]. The impact parameter calculation is straightforward:

$$\begin{aligned} m &= \frac{r_3 - r_1}{z_3 - z_1} \\ b &= r_1 - m z_1 \\ ip &= \frac{-b - m V_z}{\sqrt{m^2 + 1}} \end{aligned} \tag{1}$$

If the primary vertex is *not* in the centre of the VELO, $X = V_x$ and $Y = V_y$, then the straight line parametrisation of a 2d-track becomes an approximation, and the calculation of the impact parameter reads:

$$\begin{aligned} \text{Vertex} &= (V_x, V_y, V_z) = (r_0 \cos\phi_0, r_0 \sin\phi_0, V_z) \\ a^2 &= r^2 + r_0^2 - 2 r r_0 \cos(\phi - \phi_0) \\ m' &= \frac{a_3 - a_1}{z_3 - z_1} \\ b' &= a_1 - m' z_1 \\ ip' &= \frac{-b' - m' V_z}{\sqrt{m'^2 + 1}} \end{aligned} \tag{2}$$

where the variables a and b' are indicated in Fig. 3 and the subscripts 1 and 3 denote the cluster numbers.

The transverse width of the LHC beam is approximately 70 μm, and therefore the primary vertex position is close to $X = Y = 0$. In the approximation $r_0 << r_1$ the following expression of the 2d impact parameter is obtained (see Fig. 4):

$$\begin{aligned} a &= r\sqrt{1 + \frac{r_0^2}{r^2} - \frac{2 r_0}{r}\cos(\phi - \phi_0)} \\ &\sim r(1 + \frac{r_0^2}{2r^2} - \frac{r_0}{r}\cos(\phi - \phi_0)) \sim r - r_0 \cos(\phi - \phi_0) \\ m' &= m \\ b' &= b - r_0 \cos(\phi - \phi_0) \\ ip_{\,Y} &= \frac{-b - m V_z + r_0 \cos(\phi - \phi_0)}{\sqrt{m^2 + 1}} \end{aligned} \tag{3}$$

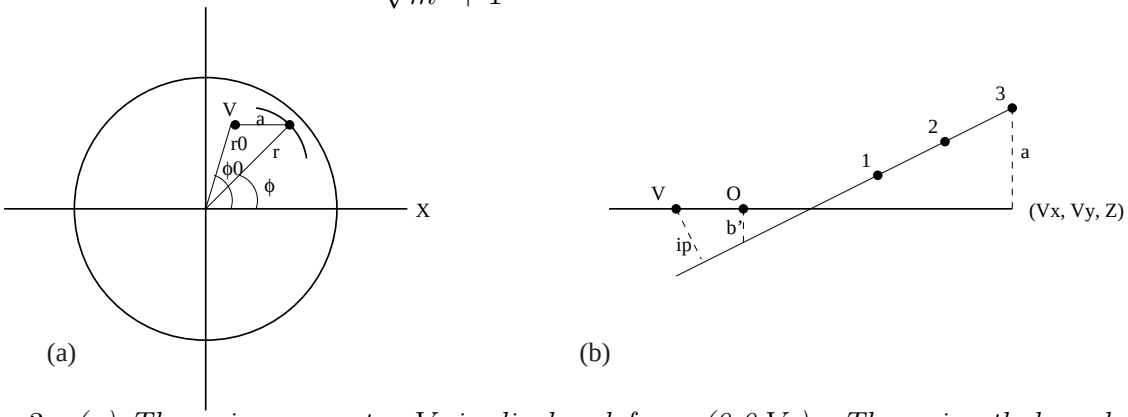

Figure 3: *(a) The primary vertex V is displaced from (0,0,V_z). The azimuthal angles of the clusters of the triplet, ϕ, and of the vertex, ϕ_0, are indicated. (b) The 2d-track is "forced" to cross the axis (V_x, V_y, V_z). The three clusters forming a triplet are also indicated.*

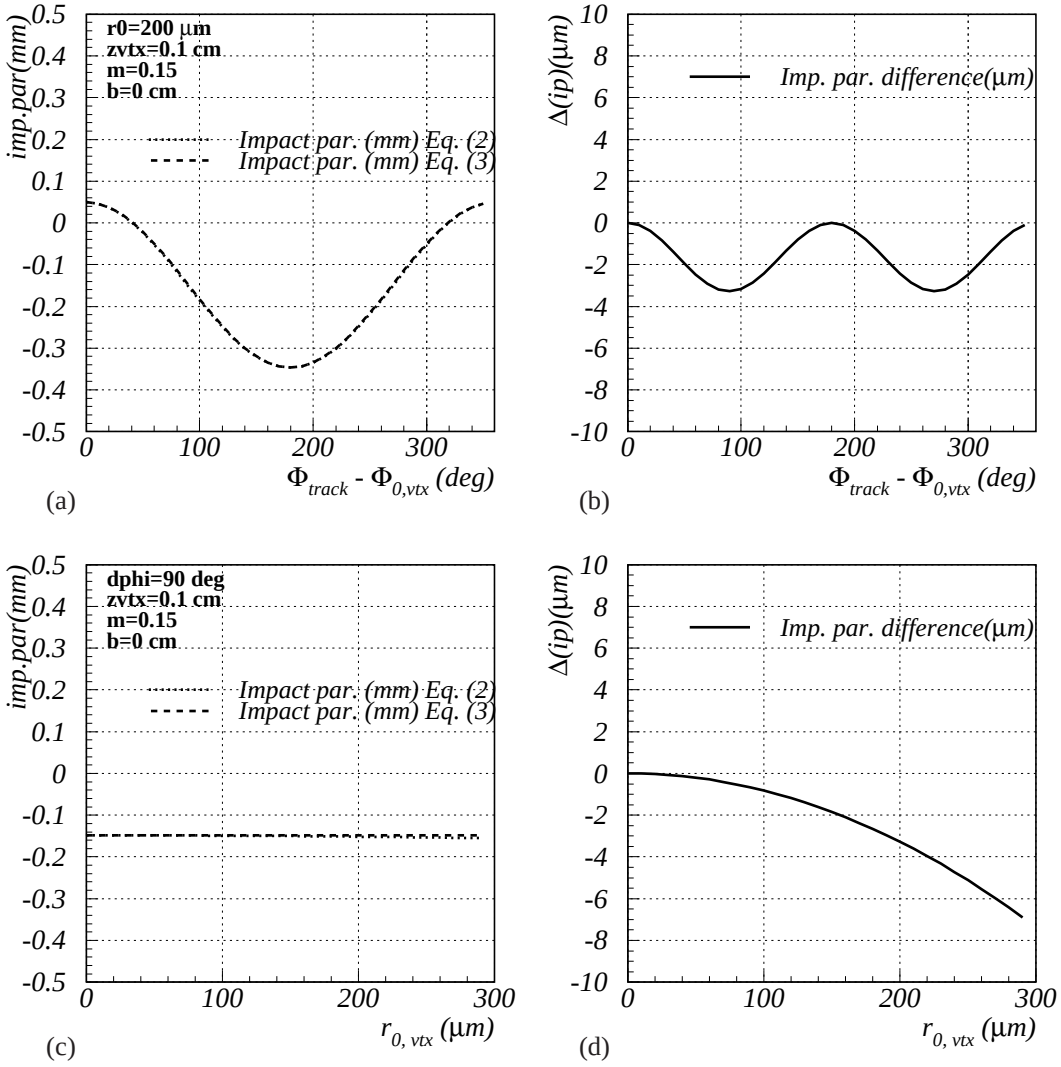

Figure 4: *The value of the 2d impact parameter is shown as calculated in Eq. (2) and in the approximation from Eq. (3), as a function of* $\phi - \phi_0$ *(a) and as a function of* r_0 *(b) respectively. (c-d) The difference between the calculations is also shown. The two calculations are identical if the primary vertex is reconstructed on the z-axis,* $r_0 = 0$*, or if the primary vertex is displaced in the plane defined by the z-axis and the 2d-track,* $\phi - \phi_0 = 0$ *or* 180^o*.*

4 Results of re-tuning

In this section the results will be shown after the retraining of all 1+5+6+3 neural nets. The inputs for the tuning of the neural nets is described in detail elsewhere [1]. The results of the retraining are given in this section, and can be compared to the results obtained with the TP geometry.

The re-tuning of the b-probability for 2d-tracks is shown in Fig. 5. The information to calculate the difference between the angle of the last measured point and the angle of the triplet closest to the primary vertex (a measure for the multiple scattering angle), was not available. In future studies this variable can be replaced by the χ^2 of the 2d-track, providing a different, more powerful measure of the multiple scattering angle. The number of minimum bias tracks at high output values have increased due to the broadening of the impact parameter distribution.

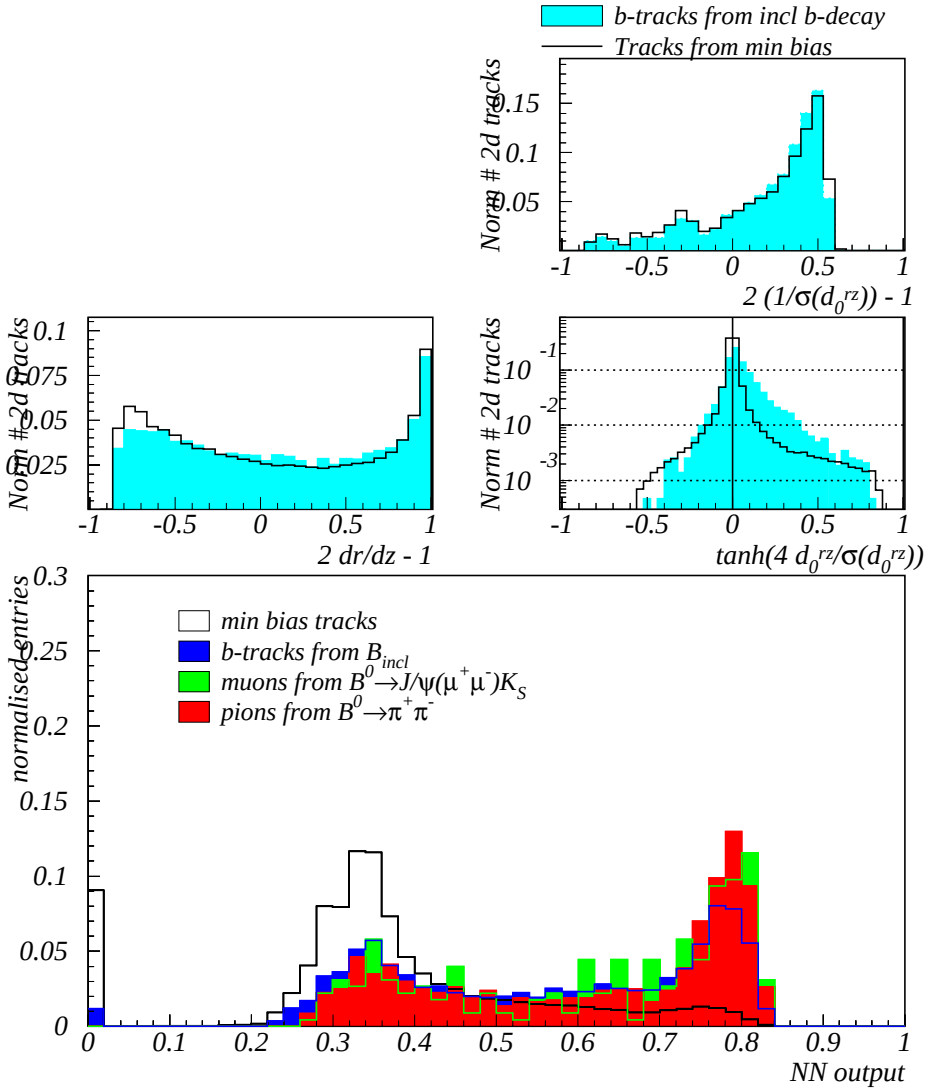

Figure 5: *The inputs are shown that are used to determine the b-probability of a 2d track. The outputs for minimum bias and signal (b-inclusive, $B^0_d \to J/\Psi(\mu^+\mu^-)K_S$ and $B^0_d \to \pi^+\pi^-$ respectively) are also shown.*

The 2d-tracks with b-probability > 0.5, or the 2d-tracks that are matched to a L0 object, are reconstructed in 3d. These 3d tracks are then again matched to a L0 object. The probabilities for 5 different matched-track hypotheses are assigned to a matched object, see Fig. 6.

- matched muon in an inclusive b-event
- matched electron in an inclusive b-event
- matched hadron in an inclusive b-event
- matched muon in a $B_d^0 \to J/\Psi(\mu^+\mu^-)K_S$ event
- matched hadron in a $B_d^0 \to \pi^+\pi^-$ event

The matched-electron neural net in inclusive b-events has *not* been retrained due to low statistics. In 1163 inclusive b-events, a total of 1654 electron-VELO matches are found. Only 36 matches originate from a B-meson, are correctly matched *and* pass the selection. The neural net from the TP study is used.

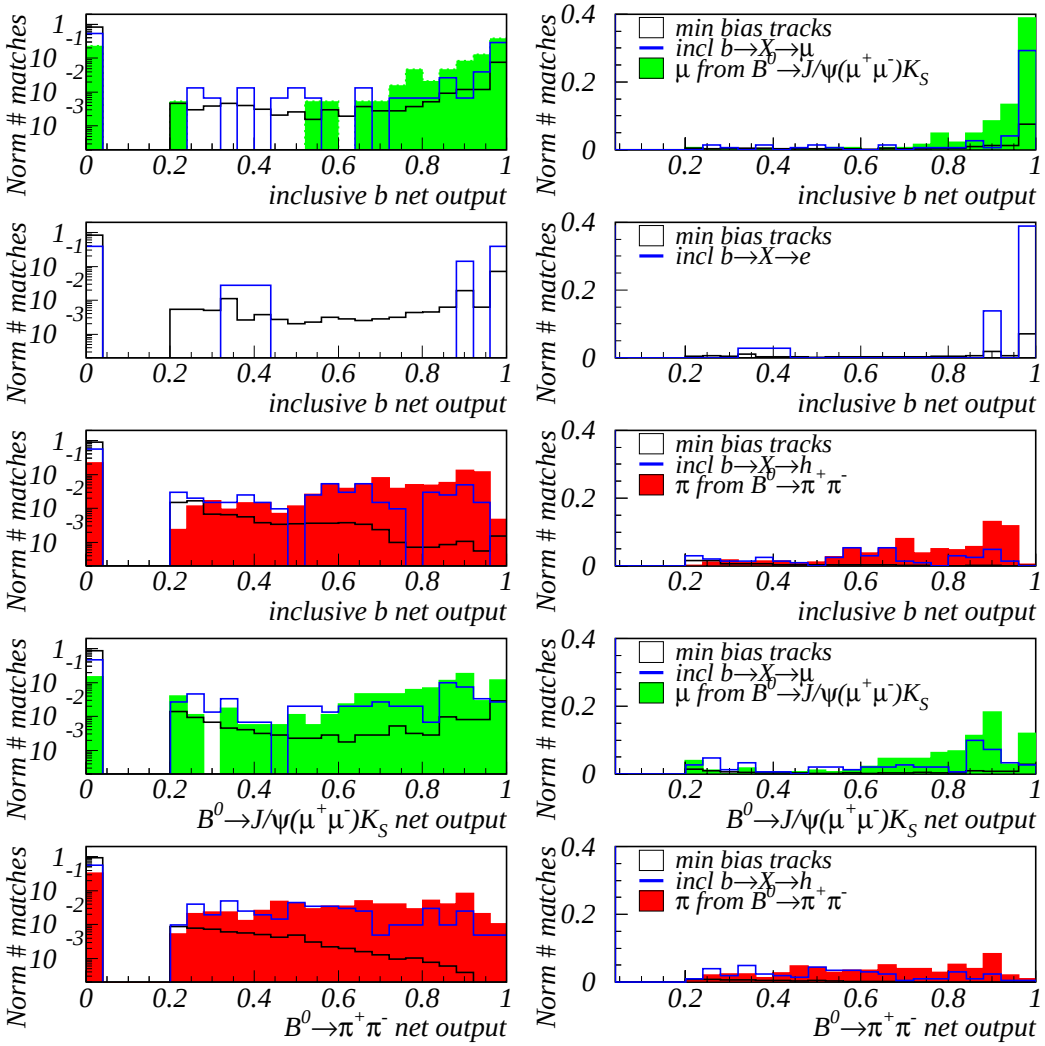

Figure 6: *The outputs (i.e. the b-probabilities) for the 5 different matched-track hypotheses are shown, both on a logarithmic (left) and on a linear sale (right).*

Subsequently, 3d-tracks are selected to form two-track vertices. Six types of two-track vertices are considered, and the corresponding b-probabilities are shown in Fig. 7.

- 2 matched muons in a $B^0_d \to J/\Psi(\mu^+\mu^-)K_S$ event.
- matched muon and an unmatched track in a $B^0_d \to J/\Psi(\mu^+\mu^-)K_S$ event.
- matched L0 object and an unmatched track in an inclusive b-event.
- 2 unmatched tracks in an inclusive b-event.
- matched hadron and an unmatched track in a $B^0_d \to \pi^+\pi^-$ event.
- 2 unmatched tracks in a $B^0_d \to \pi^+\pi^-$ event.

The category "two unmatched tracks in an inclusive b-event" has least discriminative power. The selection of these events relies on tracks with large impact parameter.

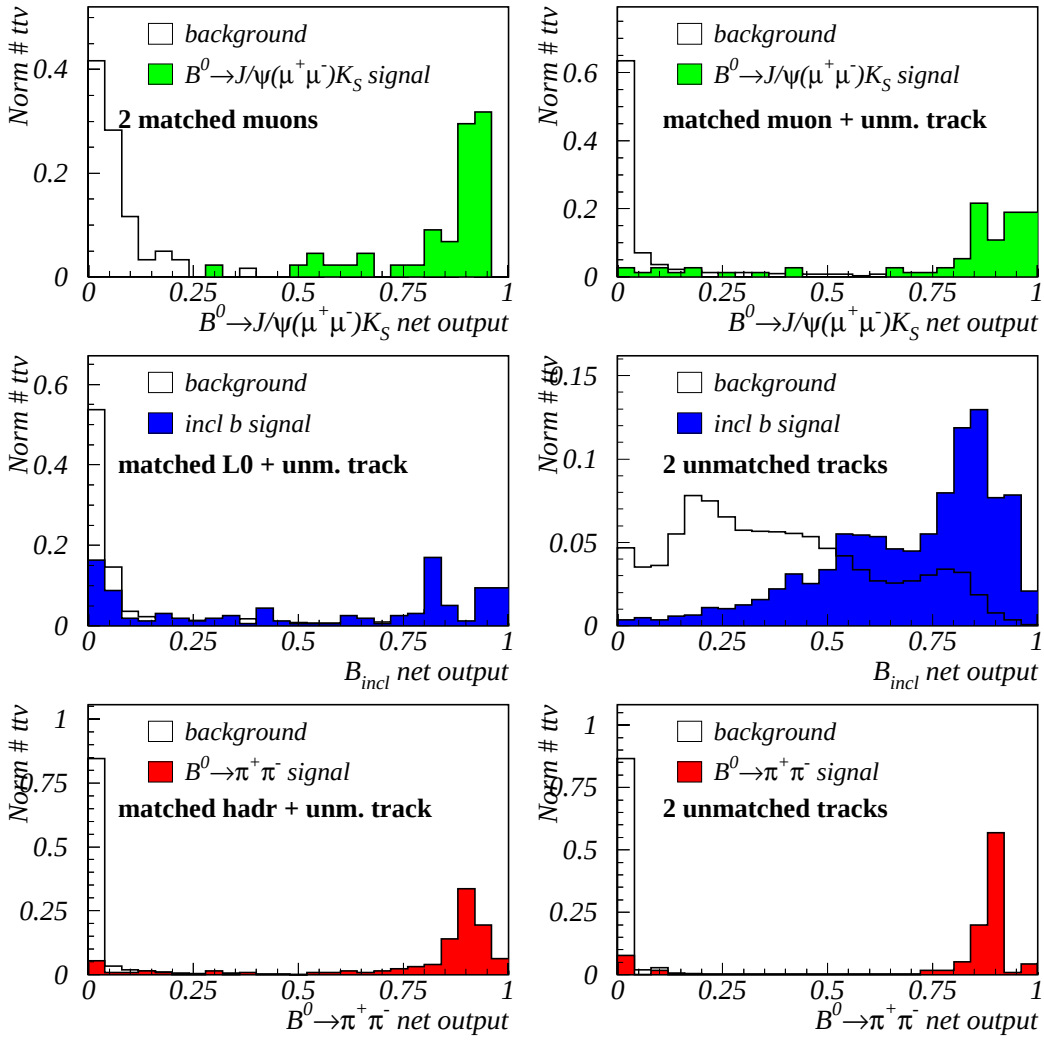

Figure 7: *The outputs (i.e. the b-probabilities) for the 6 different two-track vertex hypotheses are shown.*

Three b-probabilities, belonging to the three signal hypotheses (inclusive b-decays, $B^0_d \to J/\Psi(\mu^+\mu^-)K_S$ and $B^0_d \to \pi^+\pi^-$), are assigned to each event. The b-probability distributions of 2d-tracks, matched tracks and two-track vertices are used as inputs. The maximum value of these three probabilities is the final event probability, and is used in the decision unit to select the signal events. The event probability for each b-decay channel is shown in Fig. 8. The events that contain no 2d tracks with b-probability > 0.5 populate the first bin with negative event probability.

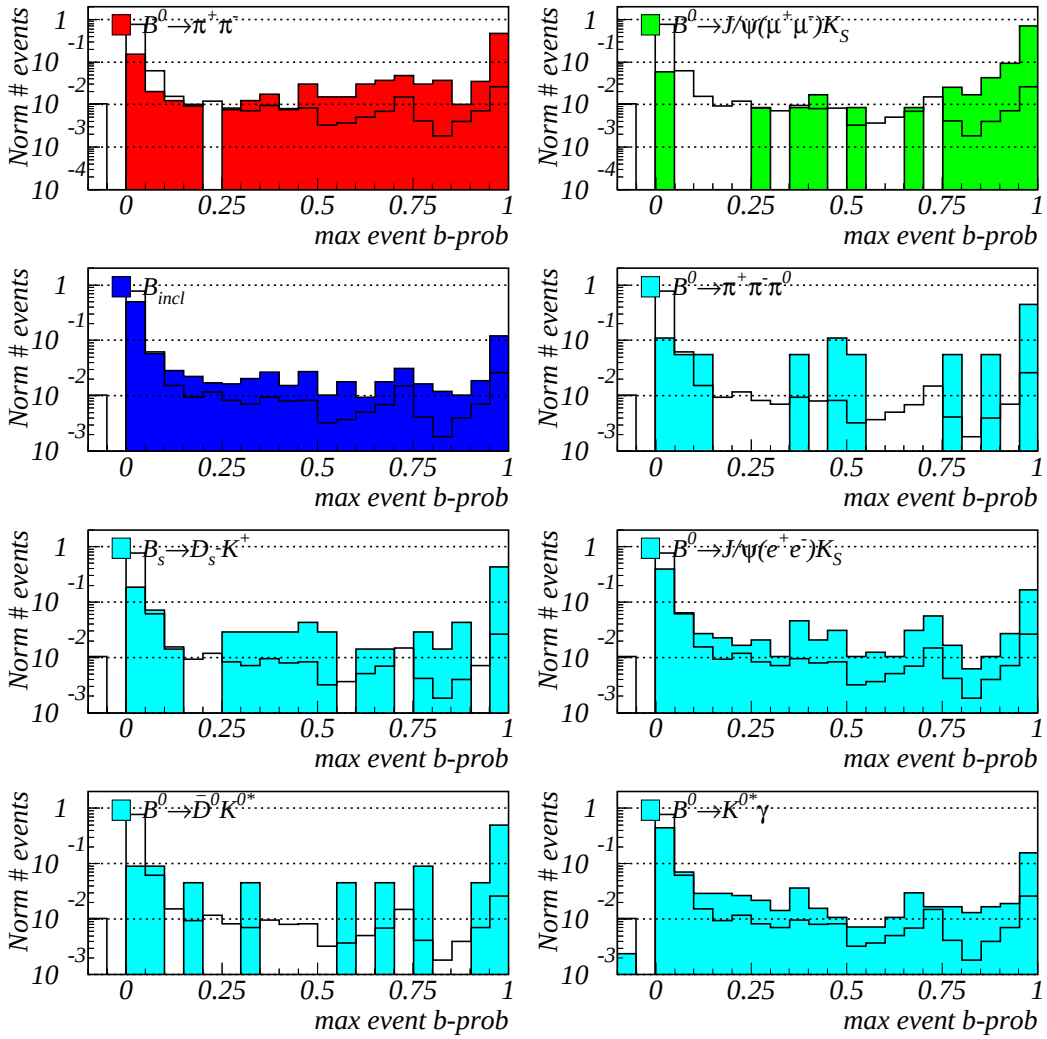

Figure 8: *The event probability is shown for each decay channel separately. The event probability is the maximum value of the 3 different values of the 3 hypotheses. The open histogram represents the event probability for minimum bias events, and is identical for all plots.*

5 Performance

The signal efficiency versus minimum bias retention is shown in Fig. 9. The L0 output rate is 1 MHz, whereas the output rate of L1 is 40 kHz. A minimum bias retention of 4% therefore corresponds to the maximum output rate of 40 kHz. The efficiency to select signal events is defined with respect to the offline (AXSEL) physics selection. The two decay channels $B_d^0 \to K^{0*}\gamma$ and $B_d^0 \to J/\Psi(e^+e^-)K_S$ show a relatively low efficiency of around 20% at an output rate of 40 kHz. This is due to the absence of AXSEL selection criteria for these channels, see Table 5.

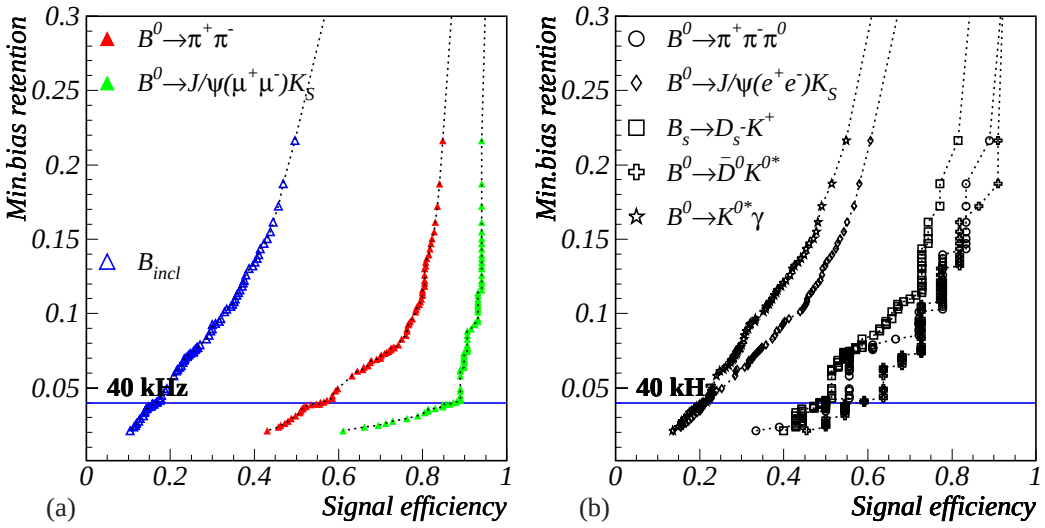

Figure 9: *(a) The minimum bias retention is shown as a function of the signal efficiency for two decay channels and for the inclusive b-decay sample. (b) The minimum bias retention versus signal efficiency is shown for five separate decay channels.*

A direct comparison between the results achieved with the TP geometry [1], and the results using the TDR geometry, is shown in Fig. 10. The SL1 performance of the multi-decay channel degraded most, with respect to the TP study. This can be understood by the fact that the B-inclusive events strongly rely on the presence of large impact parameter

Decay channel	Efficiency	AXSEL level
$B_d^0 \to X$	15%	x
$B_d^0 \to \pi^+\pi^-$	55%	2
$B_d^0 \to J/\Psi(\mu^+\mu^-)K_S$	90%	2
$B_d^0 \to \pi^+\pi^-\pi^0$	50%	1
$B_d^0 \to \overline{D}^0 K^{0*}$	60%	2
$B_s^0 \to D_s^{\pm} K^{\mp}$	50%	2
$B_d^0 \to J/\Psi(e^+e^-)K_S$	20%	0
$B_d^0 \to K^{0*}\gamma$	20%	0

Table 5: *Signal efficiencies are listed for various decay channels at an L1 output rate of 40 kHz.*

tracks. Due to the increase in dead material in the TDR geometry, with respect to the TP geometry, the number of minimum bias events with large impact parameter tracks has increased, see Fig. 2. The channels $B_d^0 \to J/\Psi(\mu^+\mu^-)K_S$ and $B_d^0 \to \pi^+\pi^-$ are less affected due to the presence of a high P_T hadron and a muon respectively, that can distinguish between minimum bias and signal events.

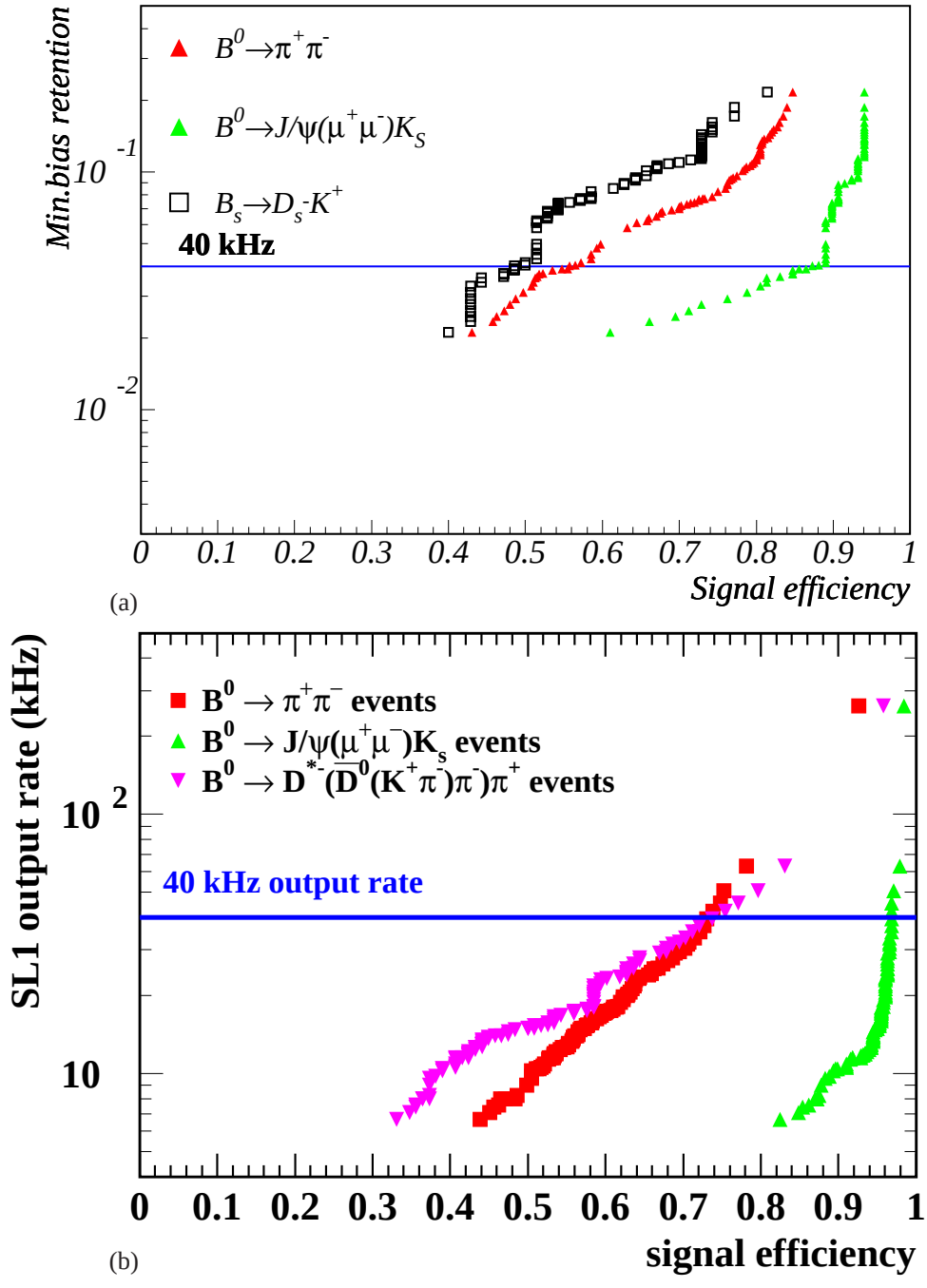

Figure 10: *(a) The minimum bias retention is shown versus the signal efficiency. The neural nets are retrained with the TDR geometry. (b) The minimum bias retention versus retention plot is shown as was obtained with the TP geometry [1].*

6 Summary

The Super Level 1 algorithm, using a more realistic detector geometry as described in the various TDR reports, achieves acceptable performance. However, the signal efficiency has deteriorated with respect to the performance obtained with the TP geometry. This is mainly caused by the increase of the amount of dead material between the VELO sensors and the primary vertex. The matching of VELO tracks with muon candidates from L0 however provides a powerful tool to efficiently select B-events with muons as decay products.

7 Acknowledgements

All the work described in this note is based on the initial work by Frank Fiedler. I would like to thank him very much for the nice cooperation, the smooth taking over of SL1 and the enormous support in understanding the algorithm.

References

[1] F. Fiedler, *Super-Level1* LHCb 2002-012 TRIG (Mar 2002).

[2] H. Dijkstra and T. Ruf, *The L1 vertex trigger algorithm and its performance* LHCb 1998-006 TRIG (Jan 1998).

[3] The LHCb Collaboration, *LHCb Technical Proposal*, CERN/LHCC 98-4 (1998).

[4] The LHCb Collaboration, *Vertex Locator Technical Design Report*, CERN/LHCC 2001-011 (May 2001).

[5] The LHCb Collaboration, *Muon System Technical Design Report*, CERN/LHCC 2001-010 (May 2001).

[6] The LHCb Collaboration, *Calorimeters Technical Design Report*, CERN/LHCC 2000-0036 (Sep 2000).

[7] T. Ruf, *VELO light workshop*, VELO meeting, (Nov 2001).

[8] R. Richter, *Implementierung eines Algorithmus für den LHCb Level-1 vertex-trigger*, CERN-THESIS-2001-001 (2000).

[9] H. Dijkstra, *TDR schedule*, Trigger meeting, LHCb coll. meeting, Rio de Janeiro (Sep 17, 2001).

[10] H. Dijkstra, *L0 Trigger rates*, Trigger meeting, LHCb coll. meeting, (Dec 2001).

[11] G. Corti, *Status of AXSEL library and first release of DaVinci*, Physics Task Force meeting (July 2001).

[12] Y. Ermoline et al., *LHCb Level-1 vertex topology trigger*, LHCb 99-031 (Aug 1999).

[13] Y. Ermoline, *Vertex detector electronics: L1 electronics system issues*, LHCb 2001-124 VELO (Oct 2001).